

pubs.acs.org/JCTC Article

Determination of Equilibrium Adsorbed Morphologies of Surfactants at Metal-Water Interfaces Using a Modified Umbrella Sampling-Based Methodology

Himanshu Singh and Sumit Sharma*



Cite This: https://doi.org/10.1021/acs.jctc.2c00078



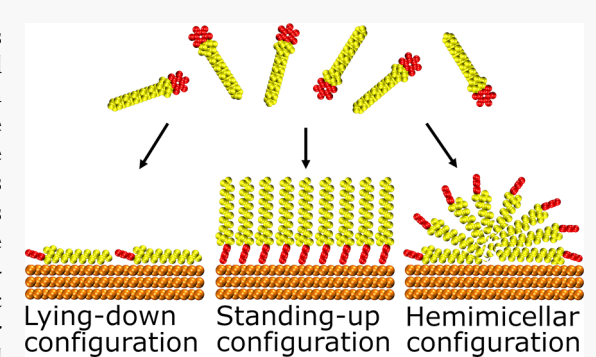
ACCESS

Metrics & More

Article Recommendations

Supporting Information

ABSTRACT: Surfactants adsorb to metal-water interfaces in various morphologies, including self-assembled monolayers (SAMs), cylindrical and spherical micelles, or hemimicelles. Current molecular simulation methods are unable to efficiently sample the formation of these morphologies because of the large diffusive/energetic barriers. We introduce a modified umbrella sampling-based methodology that allows sampling of these morphologies from any initial configuration and provides free energy differences between them. Using this methodology, we have studied adsorption behavior of cationic [quaternary ammonium (quat) of 4 and 12 carbon long alkyl tails], uncharged [decanethiol], and anionic [phosphate monoester] surfactants and their mixtures at a gold-water interface. We find that while Coulombic repulsion between the charged head groups of quat-4 limits their adsorption to a sparse layer, stronger



hydrophobic interactions between the alkyl tails of quat-12 promote adsorption resulting in a morphology with adsorbed hemispherical micelles sitting atop a monolayer. Decanethiol molecules adsorb in a densely packed bilayer with the molecules standing-up on the surface in the first layer and lying parallel to the surface in the second layer. Cationic and anionic surfactant mixtures display a synergistic adsorption behavior. These results elucidate the role of molecular characteristics in dictating the nature of adsorbed morphologies of surfactants at metal-water interfaces.

1. INTRODUCTION

Understanding surfactant-metal interactions is important for numerous applications, including corrosion inhibition, improving selectivity of chemical reactions in heterogeneous catalysis,² synthesis of anisotropic metallic nanoparticles,³ and modulating electrochemical reactions. Surfactants have a strong affinity to adsorb at metal-water interfaces and display a rich adsorption behavior as a function of their molecular properties. As an example, increasing the alkyl tail length of cetyltrimethylammonium bromide (CTAB) during the CTAB-mediated synthesis of gold nanorods increases the aspect ratio of the nanorods, presumably because longer alkyl tails cause stronger intertail packing in the adsorbed CTAB layer. In the synthesis of gold nanorods, increasing the size of the polar head of surfactants has shown to enhance the anisotropy of the nanorods. Indeed, direct scanning of morphologies of adsorbed surfactants on metallic and polar surfaces has revealed the formation of planar, spherical,8 and cylindrical micelles.9,10 The formation of these morphologies is understood to be dictated by molecular geometry, 11,12 lateral hydrophobic interactions, 13-17 as well as Coulombic interactions between the polar head, surface, and the counterions. 8,10,16 For instance, based on the differences in the atomic force microscopy (AFM) images, Jaschke et al. postulate that the adsorption of C₁₄TAB molecules on gold is mediated by

Br $^-$ counterions resulting in cylindrical micelles, while $C_{16}TAOH$ and sodium dodecyl sulfate (SDS) adsorb as hemicylindrical micelles due to the interactions between the alkyl tails and the surface. Using sum frequency generation (SFG) microscopy, Khan et al. show that the cationic alkyl dimethyl benzyl ammonium bromide surfactants with four carbon long (C_4) alkyl tails adsorb in random orientations on a gold surface, whereas the ones with C_{12} alkyl tails adsorb in a planar SAM, thereby highlighting the importance of lateral hydrophobic interactions between the alkyl tails in the adsorption. It should be noted that in these studies, the AFM and SFG microscopy have resolutions of, at best, tens of nanometers and therefore are unable to resolve the morphologies at the atomistic scale.

While it is recognized that multiple factors influence the adsorption morphology of surfactants at metal-water interfaces, no unifying guiding principle to predict these morphologies has

Received: January 21, 2022



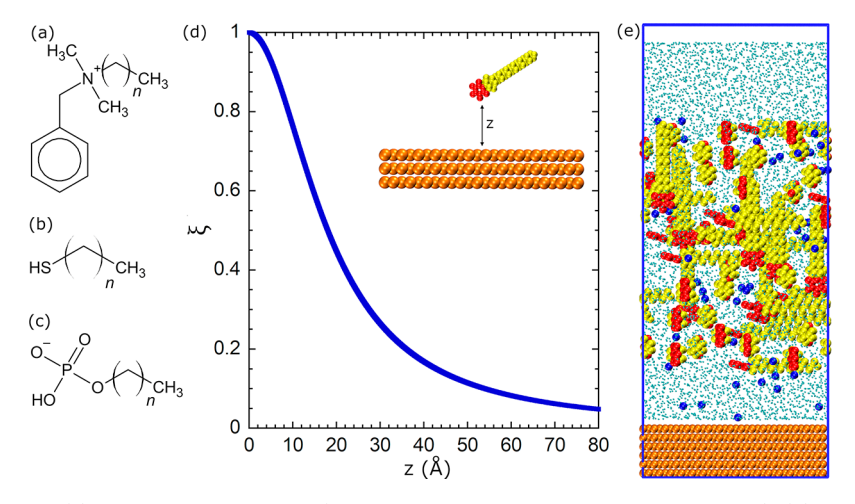


Figure 1. Molecular structures of (a) cationic quat surfactants (n = 3 and 11 for quat-4 and quat-12, respectively), (b) alkanethiol surfactant (n = 9 for decanethiol), and (c) phosphate monoester surfactant (n = 11 for pe-12). (d) $\xi(z, z_o, n, m)$ as a function of z for N = 1. The values of other parameters are $z_0 = 18$ Å, n = 2, and m = 4. (e) Initial configuration of the simulation system with quat-12 molecules near the gold-water interface. The red beads represent the aromatic rings, the yellow beads represent the alkyl tails of the surfactant molecules, the blue beads represent the bromide counterions, and the cyan dots represent water molecules. Gold atoms are shown as orange beads.

emerged so far. One reason is that the organization of surfactant molecules in densely packed adsorbed morphologies is characterized by diffusional and/or energetic barriers, and the existing molecular simulation methodologies do not allow efficient sampling of the formation of these morphologies. Previous simulation studies have attempted to navigate this problem by initializing the simulations with surfactants arranged in a planar SAM on surfaces. This approach is suboptimal as it introduces a bias toward certain configurations and does not allow calculation of the free energy of adsorbed morphologies to determine the most stable one. In this work, we introduce a new umbrella sampling-based free energy sampling methodology that allows study of densely packed adsorbed morphologies. Using this methodology, we have determined the most stable adsorbed morphology of different surfactant molecules.

2. THEORY AND SIMULATION METHODOLOGY

We have performed molecular dynamics (MD) simulations to study the adsorption behavior of cationic quaternary ammonium-based molecules of alkyl tail lengths, C_4 and C_{12} [henceforth referred to as quat-4 and quat-12, respectively], charge-neutral decanethiol, and anionic phosphate monoester molecules of C_{12} alkyl tail length [henceforth referred to as pe-12] at a gold-water interface. These molecules are widely used for corrosion inhibition in the oil and gas industry. The structures of these molecules are shown in Figure 1(a–c). In addition, we have studied adsorption of mixtures of these molecules. First, we introduce our free-energy methodology that allows sampling of high-density adsorption morphologies.

The equilibrium adsorption morphology of surfactant molecules is the one that has the lowest free energy among the other morphologies. One needs to come up with a collective variable along which one can sample different adsorption morphologies. For this purpose, we define an *adsorption number* function given by

$$\xi(z, z_o, n, m) = \sum_{i=1}^{N} \frac{1 - (z_i/z_o)^n}{1 - (z_i/z_o)^m}$$
(1)

where z_i is the distance of the polar head of the surfactant molecule identified by the subscript i from the top layer of the

metal lattice; z represents the set of z_i for all i; z_o is the cutoff distance that decides the point of inflection of the function; n and m are integers (n < m) that control the long-range behavior and stiffness of the function; and N is the total number of surfactant molecules in the system. As $z \to 0$, $\xi(z, z_o, n, m) \to N$, and as $z \to \infty$, $\xi(z, z_o, n, m) \to 0$. Therefore, $\xi(z, z_o, n, m)$ maps the number of adsorbed molecules to a continuous and differentiable function with the range of (0, N]. The departure from using integers (number of adsorbed molecules) to using a continuous and differentiable function to represent the adsorbed amount is advantageous, as one can define a biased umbrella sampling potential based on $\xi(z, z_0, n, m)$ that does not change stepwise, and therefore, the biasing forces are well-defined. The strategy of transforming discrete collective variables to differentiable functions has been utilized in prior works, for example, in a study of folding of Trp-Cage protein²⁶ and in the Indirect Umbrella Sampling methodology introduced by the Patel group.²⁷ To the best of our knowledge, ours is the first study wherein this strategy has been applied to study adsorption morphologies of molecules at interfaces. For our system, we select $z_0 = 18$ Å, n = 2, and m = 4. For ease of representation, we simply refer to the adsorption number function as ξ . For a single molecule (N = 1), the dependence of ξ on z is shown in Figure

To sample different adsorbed amounts, we apply an umbrella sampling bias potential based on ξ given by $U(\xi, \xi_o) = \frac{1}{2}k(\xi - \xi_o)^2$, where k is the force constant; ξ is the value of the adsorption number function for a configuration; and ξ_o is the set value of the adsorption number function for an umbrella sampling window. After sampling all the windows, the free energy profile as a function of ξ is generated by applying the weighted histograms analysis method. The umbrella sampling is performed using the COLVARS package in LAMMPS. The initial configurations of our MD simulation are generated by inserting the surfactant molecules at random locations and orientations in the simulation box [Figure 1(e)].

The simulation box is periodic in the X and Y directions, and a metal surface comprising of six layers of gold atoms arranged in (111) Miller index occupies the z=0 face of the simulation box. The opposite face of the simulation box has an athermal

reflective wall. A vacuum region of ~10 Å is kept above the water column to ensure that the system pressure remains at the saturation pressure corresponding to $T = 300 \text{ K.}^{31}$ To prevent the surfactant molecules from accumulating at the air-water interface, 18 we place a barrier in the form of a wall at ~ 15 Å below the air-water interface, which is permeable to the water molecules but not to the surfactant molecules and counterions. The top three layers of the gold lattice are mobile, whereas the bottom three layers are immobile. Area of the gold surface exposed to the aqueous medium, equal to the x-y dimensions of the simulation box, is 49.04 Å \times 49.97 Å. Partial charge on each atom of a surfactant molecule is calculated from density functional theory (DFT) calculations using B3LYP hybrid functional theory with the 6-31G(d,p) basis set in implicit water using Gaussian 16.32 Interaction potential parameters of surfactant molecules are obtained from the General Amber Force Field (GAFF).³³ Water molecules are represented using the extended simple point charge (SPC/E) model.³⁴ Interaction potential parameters of gold atoms are obtained from the interface force field developed by Heinz and co-workers.3 Bromide and sodium ions are introduced as the counterions for the cationic and the anionic surfactant molecules, respectively, and their interaction potential parameters are obtained from Joung and Cheatham's model.³⁶ The overall system is chargeneutral. The gold-thiol interaction is obtained from a previous work.³⁷ The cutoff distances for Lennard-Jones and short-range Coulombic interactions are taken as 10 Å. The long-range Coulombic interactions are calculated using the particleparticle particle mesh (pppm) method. The simulations are performed in the canonical ensemble (constant number of particles N, volume V, and temperature T) at a temperature of 300 K.

We have employed the above-described umbrella sampling methodology to study the equilibrium adsorption morphology of five different surfactant systems—quat-12, quat-4, decanethiol, an equimolar mixture of quat-12 and pe-12, and an equimolar mixture of quat-12 and quat-4. All simulations are performed with the same molar concentration of surfactants. In each umbrella sampling window, the system is equilibrated for the first 40 ns, and the next 40 ns are used for free energy calculations. More details of the umbrella sampling parameters and simulation system sizes are discussed in the Supporting Information.

3. RESULTS AND DISCUSSION

3.1. Adsorption of Quat-12 Molecules. The free energy profile, ΔF as a function of ξ of quat-12 molecules, is shown in Figure 2(a).

The minimum in the ΔF is observed at $\xi=27.5$, which corresponds to the most stable adsorbed morphology. A long (275 ns) unbiased MD simulation at $\xi=27.5$ does not drift away to any other value of ξ [Figure S1, Supporting Information]. The equilibrium morphology comprises of a layer of molecules lying flat on the metal surface, and on top of it, a hemispherical micelle of surfactants is adsorbed [Figure 2(b)]. The top view shows that the metal surface is nearly fully covered by the quat-12 molecules. Due to the long alkyl tails, quat-12 molecules have strong hydrophobic interactions among themselves. The ΔF is shown only for the range of $18 < \xi < 43$, as beyond this range, the $\Delta F > 100~k_{\rm B}T$. There is a free energy barrier of $\sim 4~k_{\rm B}T$ at $\xi=26.25$, which is associated with a micelle approaching the surface from the bulk aqueous phase [Figures S2 and S3, Supporting Information]. In our previous work, we have shown that a

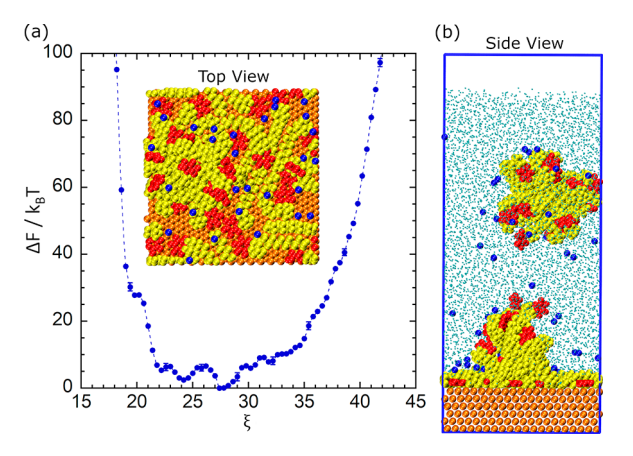


Figure 2. (a) Free energy profile, ΔF as a function of the adsorption number function, ξ , of quat-12 molecules near the metal-water interface. The inset image shows the top view of the equilibrium adsorption morphology corresponding to the free energy minimum. (b) Side view of the equilibrium adsorption morphology. Error bars in (a) are obtained from three independent estimates of the free energy profile.

cationic micelle encounters a free energy barrier to adsorption when it approaches the metal surface. $^{38-40}$ In the bulk phase, quat-12 molecules are stable in a micellar state, due to the favorable micellization free energy. 41

Figure 3(a) shows distribution of orientation of the alkyl tails of adsorbed quat-12 molecules with respect to the surface normal in the equilibrium adsorbed morphology. The angle θ is defined as the angle between the end-to-end vector of the alkyl tails and the surface normal. The cartoons shown in the inset explain the various features of the distribution. The peak at $\theta \approx$ 90° corresponds to the adsorbed monolayer of lying-down molecules. The broad plateau for $\theta \in (90^{\circ}, 180^{\circ})$ shows that the adsorbed micelle is hemispherical in shape as shown in the inset. Therefore, in the equilibrium adsorbed morphology, the quat-12 molecules adsorb as a hemispherical micelle sitting on top of a monolayer of lying-down molecules. Figure 3(b) shows distribution of the orientation of the aromatic rings of the adsorbed quat-12 molecules with respect to the surface normal, where φ is the angle between the surface normal and the vector normal to the plane of the aromatic ring. The peak at φ < 15° is due to the lying-down molecules wherein the aromatic ring is parallel to the surface. The uniform distribution for $\varphi \in (30^{\circ},$ 90°) is from the hemispherical micelle.

Due to diffusive barriers, the equilibrium adsorbed morphology is not attained in an unbiased MD simulation [Figure S4(a), Supporting Information]. Other morphologies, such as a monolayer of molecules lying parallel to the surface [Figure S4(b), Supporting Information, with $\xi_0 = 20$] or a monolayer of molecules standing-up on the surface [Figure S4(c), Supporting Information, with $\xi_0 = 47$], are free-energetically unfavorable. [Also, refer to Table S1, Supporting Information, for comparison of ensemble-average energies of the equilibrium configuration and standing-up configuration.]

3.2. Adsorption of Quat-4 Molecules. Figure 4(a) shows the free energy profile, ΔF of quat-4 molecules as a function of ξ . The equilibrium morphology corresponding to the free energy minimum at $\xi=24$ is shown in Figure 4(b). Unlike the quat-12 molecules, quat-4 molecules do not aggregate in the bulk to form micelles because of their smaller alkyl tails. The quat-4 molecules adsorb by lying flat onto the metal surface and do not completely cover the surface. There are \sim 19 quat-4 molecules adsorbed in

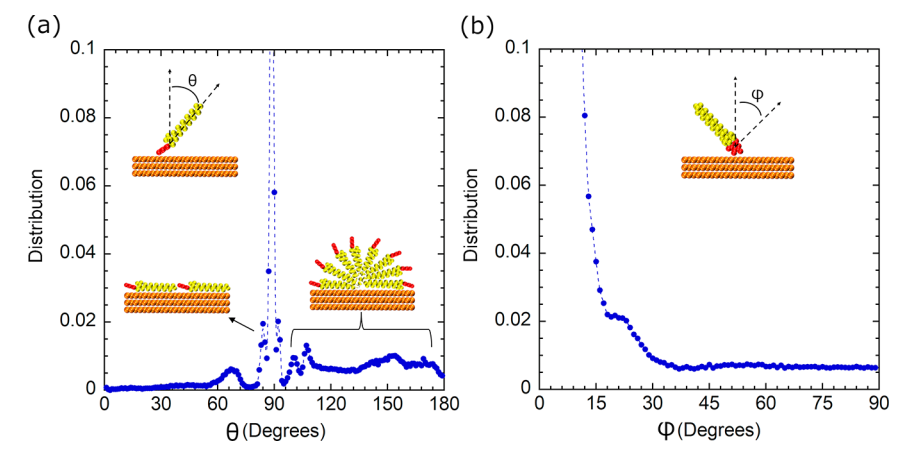


Figure 3. Distribution of the orientation of (a) alkyl tails and (b) aromatic rings of adsorbed quat-12 molecules on the metal surface. In (a), θ is the angle between the end-to-end vector of the alkyl tails and the surface normal. In (b), φ is the angle between vectors normal to the aromatic ring and the surface normal. The distribution profiles are normalized by $\langle N \rangle \sin(\theta)$ and $\langle N \rangle \sin(\varphi)$, respectively, where $\langle N \rangle$ is the ensemble-average number of adsorbed molecules. A molecule is considered as adsorbed when its center-of-mass lies within one molecular length (~23 Å) from the metal surface. The height of the adsorbed hemispherical micelle is around one molecular length. In (b), a large peak for $0^{\circ} < \varphi < 15^{\circ}$ indicates that for the molecules lying down on the surface, the aromatic rings are parallel to the metal surface. The uniform distribution observed for $30^{\circ} < \varphi < 90^{\circ}$ is from the adsorbed hemispherical micelle.

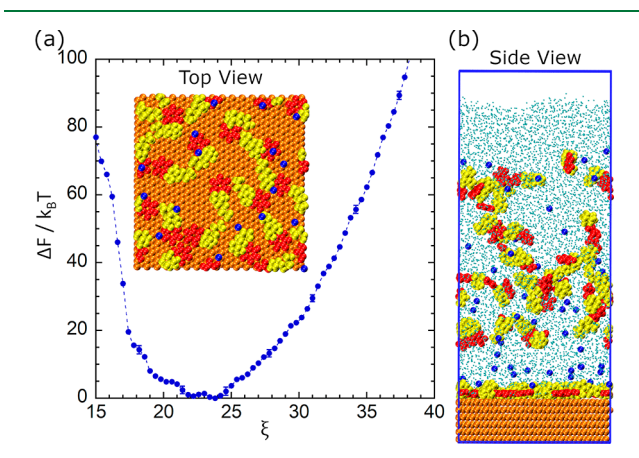


Figure 4. (a) Free energy profile, ΔF as a function of the adsorption number function, ξ , of quat-4 molecules near the metal-water interface. The inset image shows the top view of the equilibrium adsorption morphology corresponding to the free energy minimum. (b) Side view of the equilibrium adsorption morphology. Error bars in (a) are obtained from three independent estimates of the free energy profile.

the equilibrium adsorbed morphology. The sparse adsorption of quat-4 molecules is attributed to the accumulation of charged head groups on the surface, which makes further adsorption unfavorable. The distributions of the orientation of alkyl tails and the aromatic rings of the adsorbed molecules with respect to the surface normal are shown in Figure S5 [Supporting Information].

From the contrasting adsorption behavior of quat-12 and quat-4 molecules, it is concluded that the accumulation of charge limits the adsorption of cationic surfactants. In the case of quat-12 molecules, the strong hydrophobic interactions between the alkyl tails result in a configuration wherein a hemispherical micelle adsorbs on top of a monolayer of molecules lying parallel to the surface. Interestingly, the morphology with micelles of adsorbed surfactant molecules atop a monolayer of molecules lying parallel to the surface has been proposed before based on AFM imaging. ¹⁰ Surfactant molecules with small alkyl tails (<C₆) show a significantly reduced corrosion inhibition efficiency. ^{42,43} Furthermore, sum frequency generation (SFG)

experiments performed on quat-4 adsorbed at the gold-water interface show a weakly adsorbed layer. ¹⁸ This result is rationalized by our findings that quat-4 molecules only partially cover the surface.

3.3. Adsorption of Decanethiol Molecules. Next, we study the adsorption behavior of decanethiol molecules that are charge-neutral and have a long alkyl tail. The thiol group has a strong affinity for the metal surface. The ΔF of decanethiol molecules as a function of ξ is shown in Figure 5(a), and a side-

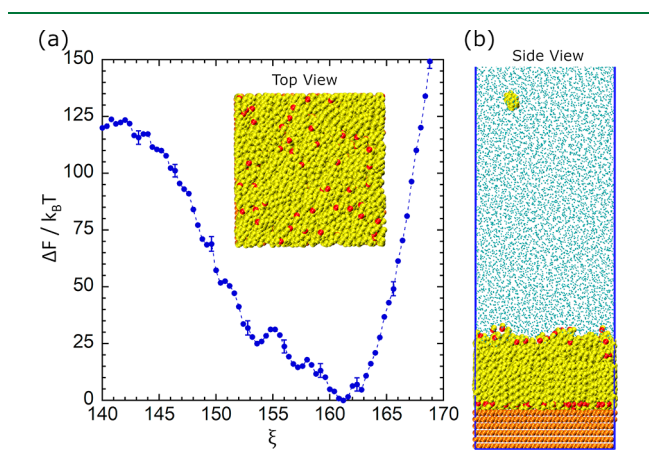


Figure 5. (a) Free energy profile, ΔF as a function of the adsorption number function, ξ , of decanethiol molecules. The inset image shows the top view of the equilibrium adsorbed morphology corresponding to the free energy minimum at $\xi=161$. (b) Side view of the equilibrium adsorbed morphology. Error bars in (a) are obtained from three independent estimates of the free energy profile. The red beads represent the thiol groups, and the yellow beads represent the alkyl tails of the molecules.

view snapshot of the equilibrium adsorbed morphology is shown in Figure 5(b). Decanethiol molecules display a much denser packing in the adsorbed state as compared to the cationic molecules. The number of adsorbed decanethiol molecules is ~ 196 as compared to ~ 30 molecules in the quat-12 system. A bilayer morphology is observed in which the first layer comprises

of the molecules aligned in a standing-up orientation on the surface, and the second layer is comprised of the molecules aligned parallel to the surface. The number of decanethiol molecules is ~147 in the first adsorbed layer and ~49 in the second adsorbed layer. The bilayer adsorption of decanethiol has also been reported in electrochemical impedance spectroscopy experiments. The distribution of the orientation of molecules in the adsorbed bilayer is shown in Figure S6 [Supporting Information]. The dense packing of decanethiol molecules on the metal surface is explained by the lack of charge accumulation, strong thiol-metal interactions, and favorable hydrophobic interactions between the alkyl tails.

3.4. Adsorption of Equimolar Mixture of Quat-12 and Pe-12 Molecules. Since the accumulation of charge is identified as a factor that limits adsorption, a mixture of cationic and anionic surfactants may show a synergistic improvement in the adsorption. To study this, we have examined adsorption behavior of an equimolar mixture of cationic quat-12 and anionic pe-12 molecules. Figure 6 shows the ΔF and the

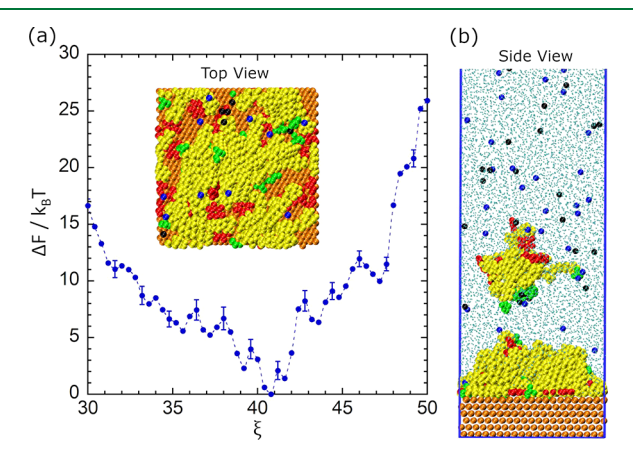


Figure 6. (a) Free energy profile, ΔF as a function of the adsorption number function, ξ , of an equimolar mixture of quat-12 and pe-12 molecules near the metal-water interface. The inset image shows the top view of the equilibrium adsorbed morphology corresponding to the free energy minimum. (b) Side view of the equilibrium adsorbed morphology. Error bars in (a) are obtained from three independent estimates of the free energy profile. The red and green beads represent the head groups of quat-12 and pe-12 molecules, respectively, and the yellow beads represent the alkyl tails of both the molecules. The blue and black beads represent the counterions: bromide and sodium ions, respectively.

corresponding equilibrium adsorbed morphology of this system. Interestingly, a significantly greater number of adsorbed molecules is observed: ~43 as compared to ~30 in a pure quat-12 system. Electrochemical measurements have previously shown that quat-14 and pe-12 molecules individually show a similar adsorption tendency. This simulation result suggests that as hypothesized, a mixture of cationic and anionic surfactant molecules shows synergistic improvement in the adsorption. The presence of oppositely charged molecules on the surface reduces the amount of charge accumulation and favors a denser adsorption morphology. The distribution of the orientation of alkyl tails of the adsorbed molecules with respect to the surface normal is shown in Figure S7 [Supporting Information].

3.5. Adsorption of Equimolar Mixture of Quat-12 and Quat-4 Molecules. We have also studied the adsorption behavior of an equimolar mixture of quat-12 and quat-4 molecules. Figure 7 shows the ΔF and the corresponding

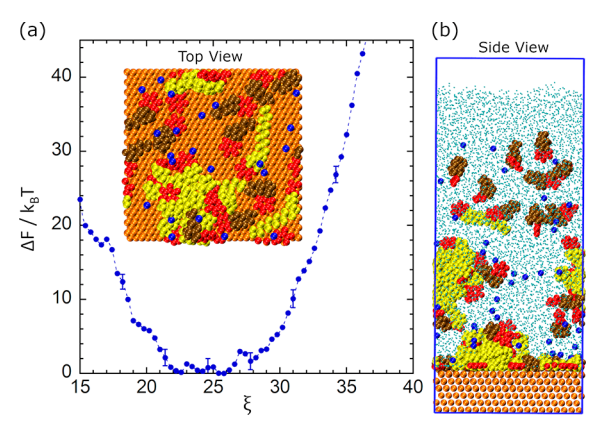


Figure 7. (a) Free energy profile, ΔF as a function of the adsorption number function, ξ , of an equimolar mixture of quat-12 and quat-4 molecules near the metal-water interface. The inset image shows the top view of the equilibrium adsorption morphology corresponding to the free energy minimum at ξ = 26. (b) Side view of the equilibrium adsorption morphology. Error bars in (a) are obtained from three independent estimates of the free energy profile. The red beads represent the aromatic rings of the quat molecules. The alkyl tails of two kinds of quat molecules are differentiated by yellow and brown beads, each representing the tails of quat-12 and quat-4 molecules, respectively. Figure S18 compares the ΔF of the mixture of quat molecules with the profiles of pure quat-12 and quat-4 molecules. The ΔF of the mixture shows a broader range of ξ at the minimum, implying that many different adsorbed configurations are possible. The distributions of the orientation of alkyl tails of the adsorbed molecules with respect to the surface normal are shown in Figure S8.

equilibrium adsorbed morphology of this system. It is observed that the quat-12 molecules adsorb in the aggregated state but are not organized in a hemispherical micelle as before [Figure S8(a), Supporting Information]. The quat-4 molecules adsorb by lying parallel onto the surface [Figure S8(b), Supporting Information]. We do not observe any synergistic improvement in the adsorption behavior in this mixture.

For inhibiting corrosion, the ability of the adsorbed surfactant molecules to exclude water from the metal surface is desired. In Figure 8, we compare the density profiles of water in the absence and presence of the adsorbed morphologies of all five surfactant systems studied. It is observed that decanethiol molecules, due to their strong packing in the adsorbed state, are the most efficient in excluding water from the interface. After

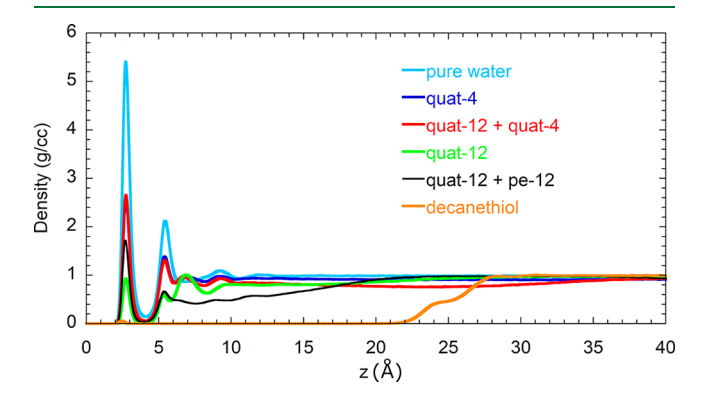


Figure 8. Density profile of water as a function of distance, *z*, from the metal surface in the absence and presence of adsorbed surfactants. Water is completely excluded from the metal surface in the case of decanethiol adsorption, whereas layers of water close to the metal surface are observed in other systems.

decanethiol, the quat-12 + pe-12 mixture comes next, followed by quat-12, quat-12 + quat-4/quat-4. This result is in agreement with prior electrochemical observations in which decanethiol molecules showed better corrosion inhibition efficiency in comparison to the quat molecules. 43,44

Since in equilibrium the adsorbed state has the same chemical potential as the bulk, increasing bulk concentration is expected to influence the adsorbed state. That said, experiments have shown that as the bulk concentration is increased, the surface concentration eventually reaches surface saturation. Further increase in the bulk concentration has no effect on the surface concentration. 48 Therefore, for the bulk concentrations larger than the surface saturation concentration, one would expect little or only nonspecific adsorption of surfactants to occur. Our simulations have been performed at the bulk concentrations above the surface saturation concentration, and we have ensured that the system is large enough that the adsorbed morphologies so obtained are not artifacts of a limited number of surfactant molecules in the system. For the quat-12 system, it will be interesting to study what happens when the systems are large enough that multiple micelles can adsorb on the surface. Performing atomistic level simulations of such large systems is prohibitive. Therefore, one approach would be to use a coarsegrained representation of surfactant molecules.

4. CONCLUSIONS

We introduce a new umbrella sampling-based methodology that enables the study of equilibrium adsorbed morphologies of surfactant molecules at interfaces. Using our methodology, we have compared the equilibrium adsorbed morphologies of cationic surfactants of different alkyl tail lengths (quat-12 and quat-4), an uncharged surfactant (decanethiol), a mixture of cationic and anionic surfactants (quat-12 and pe-12), and a mixture of quat-12 and quat-4 surfactants. Our results show that cationic surfactants with small alkyl tail lengths (quat-4) attain only partial coverage of the surface with the molecules lying parallel to the surface. The cationic molecules with longer tail lengths (quat-12) adsorb as micelles sitting on top of a monolayer of molecules lying parallel to the surface. In contrast to the cationic surfactants, charge-neutral decanethiol adsorbs as a self-assembled bilayer with the molecules standing up in the first layer and densely packing the surface. Mixtures of cationic and anionic surfactants show a synergistic improvement in the adsorption behavior. Overall, it is concluded that the accumulation of charge limits adsorption, whereas lateral hydrophobic interactions between the alkyl tails favor adsorption. Our simulation methodology can be employed to study many different surfactant systems and will help in providing a rational understanding of the rich adsorption behavior of surfactants on metallic, polar, and hydrophobic surfaces.

ASSOCIATED CONTENT

Supporting Information

The Supporting Information is available free of charge at https://pubs.acs.org/doi/10.1021/acs.jctc.2c00078.

Simulation details; time series of ξ from unbiased MD simulations (equilibrium morphology) [Figure S1]; snapshots of simulations biased [Figure S2]; distribution profiles of center-of-mass of quat-12 molecules as function of distance from metal surface for different values of ξ_a [Figure S3]; configurations of quat-12

molecules obtained from unbiased simulation started with random configuration and biased simulations [Figure S4]; comparison of pairwise energies (Lennard-Jones plus Coulombic) of quat-12 and quat-4 molecules equilibrium morphology and standing-up configuration [Table S1]; distribution of orientation of alkyl tails and aromatic rings of adsorbed quat-4 molecules on metal surface [Figure S5]; distribution of orientation of alkyl tails of adsorbed decanethiol molecules present in first and second layers on metal surface [Figure S6]; distribution of orientation of alkyl tails of adsorbed quat-12 and pe-12 molecules in equimolar mixture system of molecules [Figure S7]; distribution of orientation of alkyl tails of adsorbed quat-12 and quat-4 molecules in equimolar mixture system of molecules [Figure S8]; histograms of umbrella sampling simulations of quat-12 molecules [Figure S9]; free energy profile, ΔF plotted with respect to number of adsorbed molecules for quat-12 and mixture of quat-12 and pe-12 [Figure S10]; distribution of polar head groups of quat-12 molecules as function of distance from metal surface in equilibrium adsorbed and standing-up configurations [Figure S11]; distribution of terminal methyl groups of alkyl tails of quat-12 molecules as function of distance from metal surface in equilibrium and standing-up configurations [Figure S12]; distribution of head groups of quat-4 molecules as function of distance from metal surface in equilibrium adsorbed morphology and standing-up configuration [Figure S13]; distribution of terminal methyl groups of alkyl tails of quat-4 molecules as function of distance from metal surface in equilibrium adsorbed and standing-up configurations [Figure S14]; distribution of bromide counterions of quat-12 molecules as function of distance from metal surface in equilibrium and standing-up configurations [Figure S15]; distribution of bromide counterions of quat-4 molecules as function of distance from metal surface in equilibrium adsorbed and standing-up configurations [Figure S16]; distribution of thiol groups and terminal methyl groups as function of distance from metal surface in first and second adsorption layers of equilibrium adsorbed morphology of decanethiol molecules [Figure S17]; and comparison of ΔF as function of adsorption number function of quat molecules near metal-water interface [Figure S18] (PDF)

AUTHOR INFORMATION

Corresponding Author

Sumit Sharma — Department of Chemical and Biomolecular Engineering, Ohio University, Athens, Ohio 45701, United States; orcid.org/0000-0003-3138-5487; Phone: +1-740-593-1425; Email: sharmas@ohio.edu

Author

Himanshu Singh — Department of Chemical and Biomolecular Engineering, Ohio University, Athens, Ohio 45701, United States

Complete contact information is available at: https://pubs.acs.org/10.1021/acs.jctc.2c00078

Notes

The authors declare no competing financial interest.

ACKNOWLEDGMENTS

This work is supported by the National Science Foundation (NSF) CBET grant 1705817 and NSF CAREER grant 2046095. The authors thank the researchers at the Institute for Corrosion and Multiphase Technology (ICMT) for useful discussions. Computational resources for this work were provided by the Oak Ridge Leadership Computing Facility (project number CPH138), Ohio Supercomputer Center (project number PAA0031), and National Science Foundation XSEDE grant number DMR190005.

REFERENCES

- (1) Malik, M. A.; Hashim, M. A.; Nabi, F.; Al-Thabaiti, S. A.; Khan, Z. Anti-Corrosion Ability of Surfactants: A Review. *Int. J. Electrochem. Sci.* **2011**, *6* (6), 1927–1948.
- (2) Thomas, J. M.; Thomas, W. J. Principles and Practice of Heterogeneous Catalysis; John Wiley & Sons: 2014.
- (3) Johnson, C. J.; Dujardin, E.; Davis, S. A.; Murphy, C. J.; Mann, S. Growth and Form of Gold Nanorods Prepared by Seed-Mediated, Surfactant-Directed Synthesis. *J. Mater. Chem.* **2002**, *12* (6), 1765–1770.
- (4) Franklin, T.; Mathew, S. The Use of Surfactants in Electrochemistry. In *Surfactants in Solution*; Springer: New York, NY, 1989.
- (5) Gao, J.; Bender, C. M.; Murphy, C. J. Dependence of the Gold Nanorod Aspect Ratio on the Nature of the Directing Surfactant in Aqueous Solution. *Langmuir* **2003**, *19* (21), 9065–9070.
- (6) Kou, X.; Zhang, S.; Tsung, C.-K.; Yeung, M. H.; Shi, Q.; Stucky, G. D.; Sun, L.; Wang, J.; Yan, C. Growth of Gold Nanorods and Bipyramids Using CTEAB Surfactant. *J. Phys. Chem. B* **2006**, *110* (33), 16377–16383.
- (7) Xiong, Y.; Brown, B.; Kinsella, B.; Nešic, S.; Pailleret, A. Atomic Force Microscopy Study of the Adsorption of Surfactant Corrosion Inhibitor Films. *Corrosion* **2014**, 70 (3), 247–260.
- (8) Subramanian, V.; Ducker, W. A. Counterion Effects on Adsorbed Micellar Shape: Experimental Study of the Role of Polarizability and Charge. *Langmuir* **2000**, *16* (10), 4447–4454.
- (9) Sharma, B.; Basu, S.; Sharma, M. Characterization of Adsorbed Ionic Surfactants on a Mica Substrate. *Langmuir* **1996**, *12* (26), 6506–6512.
- (10) Jaschke, M.; Butt, H.-J.; Gaub, H.; Manne, S. Surfactant Aggregates at a Metal Surface. *Langmuir* 1997, 13 (6), 1381–1384.
- (11) Ko, X.; Sharma, S. Adsorption and Self-Assembly of Surfactants on Metal-Water Interfaces. *J. Phys. Chem. B* **2017**, *121* (45), 10364–10370
- (12) Sharma, S.; Singh, H.; Ko, X. A Quantitatively Accurate Theory to Predict Adsorbed Configurations of Linear Surfactants on Polar Surfaces. *J. Phys. Chem. B* **2019**, *123* (34), 7464–7470.
- (13) Jiménez-Ángeles, F.; Khoshnood, A.; Firoozabadi, A. Molecular Dynamics Simulation of the Adsorption and Aggregation of Ionic Surfactants at Liquid—Solid Interfaces. *J. Phys. Chem. C* **2017**, *121* (46), 25908—25920.
- (14) Ko, X.; Sharma, S. A Quantitatively Accurate Theory to Predict Adsorbed Configurations of Asymmetric Surfactant Molecules on Polar Surfaces. *J. Phys. Chem. B* **2020**, *124* (26), 5517–5524.
- (15) Sharma, S.; Ko, X.; Kurapati, Y.; Singh, H.; Nešić, S. Adsorption Behavior of Organic Corrosion Inhibitors on Metal Surfaces Some New Insights from Molecular Simulations. *Corrosion* **2019**, 75 (1), 90–105.
- (16) Zhang, R.; Somasundaran, P. Advances in Adsorption of Surfactants and Their Mixtures at Solid/Solution Interfaces. *Adv. Colloid Interfac.* **2006**, 123, 213–229.
- (17) Tariq, M.; Serro, A.; Colaço, R.; Saramago, B.; Lopes, J. C.; Rebelo, L. P. N. Effect of Alkyl Chain Length on the Adsorption and Frictional Behaviour of 1-Alkyl-3-Methylimidazolium Chloride Ionic Liquid Surfactants on Gold Surfaces. *Colloid Surface A* **2011**, *377* (1–3), 361–366.

- (18) Khan, M. R.; Singh, H.; Sharma, S.; Asetre Cimatu, K. L. Direct Observation of Adsorption Morphologies of Cationic Surfactants at the Gold Metal—Liquid Interface. *J. Phys. Chem. Lett.* **2020**, *11* (22), 9901—9906.
- (19) Meena, S. K.; Sulpizi, M. From Gold Nanoseeds to Nanorods: The Microscopic Origin of the Anisotropic Growth. *Angew. Chem-Ger. Ed.* **2016**, *128* (39), 12139–12143.
- (20) Ghorai, P. K.; Glotzer, S. C. Molecular Dynamics Simulation Study of Self-Assembled Monolayers of Alkanethiol Surfactants on Spherical Gold Nanoparticles. *J. Phys. Chem. C* **2007**, *111* (43), 15857–15862
- (21) da Silva, J. A.; Meneghetti, M. R. New Aspects of the Gold Nanorod Formation Mechanism via Seed-Mediated Methods Revealed by Molecular Dynamics Simulations. *Langmuir* **2018**, *34* (1), *366*–375.
- (22) Meena, S. K.; Sulpizi, M. Understanding the Microscopic Origin of Gold Nanoparticle Anisotropic Growth from Molecular Dynamics Simulations. *Languair* **2013**, 29 (48), 14954–14961.
- (23) Torrie, G. M.; Valleau, J. P. Nonphysical Sampling Distributions in Monte Carlo Free-Energy Estimation: Umbrella Sampling. *J. Comput. Phys.* **1977**, 23 (2), 187–199.
- (24) Hegazy, M.; Abdallah, M.; Awad, M.; Rezk, M. Three Novel Di-Quaternary Ammonium Salts as Corrosion Inhibitors for API X65 Steel Pipeline in Acidic Solution. Part I: Experimental Results. *Corros. Sci.* **2014**, *81*, 54–64.
- (25) Jovancicevic, V.; Ahn, Y. S.; Dougherty, J. A.; Alink, B. CO2 Corrosion Inhibition by Sulfur-Containing Organic Compounds. In *CORROSION 2000*; OnePetro: 2000.
- (26) Marinelli, F.; Pietrucci, F.; Laio, A.; Piana, S. A Kinetic Model of Trp-Cage Folding from Multiple Biased Molecular Dynamics Simulations. *PLoS Comput. Biol.* **2009**, *5* (8), e1000452.
- (27) Patel, A. J.; Varilly, P.; Chandler, D.; Garde, S. Quantifying Density Fluctuations in Volumes of all Shapes and Sizes using Indirect Umbrella Sampling. *J. Stat. Phys.* **2011**, *145* (2), 265–275.
- (28) Kumar, S.; Rosenberg, J. M.; Bouzida, D.; Swendsen, R. H.; Kollman, P. A. The Weighted Histogram Analysis Method for Free-Energy Calculations on Biomolecules. I. The Method. *J. Comput. Chem.* **1992**, *13* (8), 1011–1021.
- (29) Fiorin, G.; Klein, M. L.; Hénin, J. Using Collective Variables to Drive Molecular Dynamics Simulations. *Mol. Phys.* **2013**, *111* (22–23), 3345–3362.
- (30) Plimpton, S. Fast Parallel Algorithms for Short-Range Molecular Dynamics. *J. Comput. Phys.* **1995**, *117* (1), 1–19.
- (31) Patel, A. J.; Varilly, P.; Chandler, D. Fluctuations of Water Near Extended Hydrophobic and Hydrophilic Surfaces. *J. Phys. Chem. B* **2010**, *114* (4), 1632–1637.
- (32) Frisch, M.; Trucks, G.; Schlegel, H.; Scuseria, G.; Robb, M.; Cheeseman, J.; Scalmani, G.; Barone, V.; Petersson, G.; Nakatsuji, H. *Gaussian 16*, revision a.03; Gaussian, Inc.: Wallingford, CT, 2016; 2 (4).
- (33) Wang, J.; Wolf, R. M.; Caldwell, J. W.; Kollman, P. A.; Case, D. A. Development and Testing of a General Amber Force Field. *J. Comput. Chem.* **2004**, 25 (9), 1157–1174.
- (34) Berendsen, H.; Grigera, J.; Straatsma, T. The Missing Term in Effective Pair Potentials. *J. Phys. Chem.-US* **1987**, *91* (24), 6269–6271.
- (35) Heinz, H.; Vaia, R.; Farmer, B.; Naik, R. Accurate Simulation of Surfaces and Interfaces of Face-Centered Cubic Metals Using 12–6 and 9–6 Lennard-Jones Potentials. *J. Phys. Chem. C* **2008**, *112* (44), 17281–17290.
- (36) Joung, I. S.; Cheatham, T. E., III Determination of Alkali and Halide Monovalent Ion Parameters for Use in Explicitly Solvated Biomolecular Simulations. *J. Phys. Chem. B* **2008**, *112* (30), 9020–
- (37) Coppage, R.; Slocik, J. M.; Ramezani-Dakhel, H.; Bedford, N. M.; Heinz, H.; Naik, R. R.; Knecht, M. R. Exploiting Localized Surface Binding Effects to Enhance the Catalytic Reactivity of Peptide-Capped Nanoparticles. *J. Am. Chem. Soc.* **2013**, *135* (30), 11048–11054.
- (38) Singh, H.; Sharma, S. Disintegration of Surfactant Micelles at Metal—Water Interfaces Promotes Their Strong Adsorption. *J. Phys. Chem. B* **2020**, 124 (11), 2262–2267.

- (39) Singh, H.; Sharma, S. Free Energy Profiles of Adsorption of Surfactant Micelles at Metal-Water Interfaces. *Mol. Simul.* **2021**, 47 (5), 420–427
- (40) Kurapati, Y.; Sharma, S. Adsorption Free Energies of Imidazolinium-type Surfactants in Infinite Dilution and in Micellar State on Gold Surface. *J. Phys. Chem. B* **2018**, *122*, 5933–5939.
- (41) Singh, H.; Kurapati, Y.; Sharma, S. Aggregation and Adsorption Behavior of Organic Corrosion Inhibitors Studied Using Molecular Simulations. In *CORROSION 2019*; OnePetro: 2019.
- (42) Edwards, A.; Osborne, C.; Webster, S.; Klenerman, D.; Joseph, M.; Ostovar, P.; Doyle, M. Mechanistic Studies of the Corrosion Inhibitor Oleic Imidazoline. *Corros. Sci.* **1994**, *36* (2), 315–325.
- (43) Moradighadi, N.; Lewis, S.; Olivo, J. D.; Young, D.; Brown, B.; Nešić, S. Determining Critical Micelle Concentration of Organic Corrosion Inhibitors and its Effectiveness in Corrosion Mitigation. *Corrosion* **2021**, *77* (3), 266–275.
- (44) Belarbi, Z.; Dominguez Olivo, J.; Farelas, F.; Singer, M.; Young, D.; Nešić, S. Decanethiol as a Corrosion Inhibitor for Carbon Steels Exposed to Aqueous CO2. *Corrosion* **2019**, 75 (10), 1246–1254.
- (45) He, Y.; Ren, S.; Belarbi, Z.; Wang, X.; Young, D.; Singer, M.; Mohamed-Saïd, M.; Camperos, S. Micellization and Inhibition Efficiency. In *CORROSION 2021*; OnePetro: 2021.
- (46) Bergström, M.; Eriksson, J. C. Synergistic Effects in Binary Surfactant Mixtures. *Prog. Coll. Polym. Sci. S.* **2004**, 16–22.
- (47) Nešić, S. Key Issues Related to Modelling of Internal Corrosion of Oil and Gas Pipelines A Review. *Corros. Sci.* **2007**, 49 (12), 4308—4338.
- (48) Ren, S.; He, Y.; Belarbi, Z.; Wang, X.; Young, D.; Singer, M.; Mohamed-Saïd, M.; Camperos, S. Methodology for Corrosion Inhibitor Characterization Applied to Phosphate Ester and Tetrahydropyrimidinium Model Compounds. In *CORROSION* 2021; OnePetro: 2021.

